ACS Photonics

pubs.acs.org/journal/apchd5 Article

Optical Borromean Vortex Rings

Jinzhan Zhong, Renzo L. Ricca, and Qiwen Zhan*

Cite This: *ACS Photonics* 2026, 13, 1727−1733

Read Online

ACCESS | Metrics & More | Article Recommendations | Supporting Information

ABSTRACT: Borromean rings are topological objects made of three inseparable rings, where no two rings are linked with one another. Here we report the first creation of Borromean rings using three-dimensional (3D) structured light. The topological light is constructed from the homotopic mapping of complex braids, followed by the implementation of an accurate adjustment of the vortex lines in a 2D complex space. By carefully tailoring the amplitude and phase distribution of the monochromatic light, we generate the optical Borromean vortex rings within the propagation volume. Full topological reconstruction of the Borromean vortex rings is performed by using digital holography. The topological design method enables the generation of the figure-eight vortex knot family and even more complex topological textures. These findings offer insights into the topological evolution of Borromean rings in other physical systems and pave the way for potential applications in emerging technologies involving light−matter interactions, optical encoding, and quantum information.

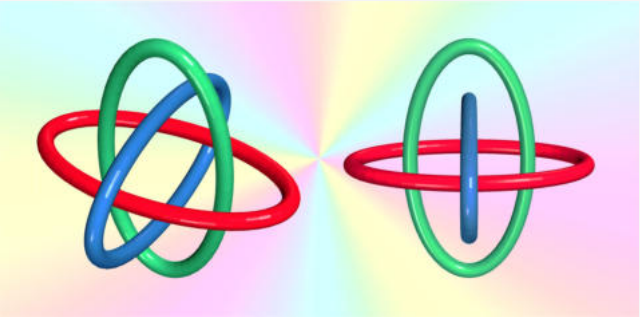

KEYWORDS: *Borromean rings, optical vortex, knot theory, structured light, topology*

INTRODUCTION

Borromean rings represent a very interesting case of topological linkage of three inseparable loops, where any pair of rings cannot be set apart from each other. They represent an essential link despite having their topological linking number equal to zero.[1] This peculiarity was already known to Maxwell, who pointed that out to Tait in a private correspondence.[2] If one of the three rings is cut open or removed, the system breaks apart into two unknotted and unlinked rings so that the integral linkage confers topological stability to the system. Different realizations of Borromean rings are shown in Figure 1 for illustration purposes: the standard mathematical representation of Borromean rings as three simple, closed tubes in space, shown in Figure 1a; the Borromean linkage of three paper clips that exposes the nonplanar feature of the system, illustrated in Figure 1b; and the Luban lock, popular in Chinese art crafts and ancient architecture, which provides an example of material stability, illustrated in Figure 1c. The topological arrangement of Borromean rings and associated physical properties find applications in different contexts, from the study of magnetic fields and liquid crystals[3,4] to quantum vortices and defects in Bose−Einstein condensates,[5,6] from DNA biology to the manufacturing of synthetic molecules,[7−10] and even in more abstract settings, from quantum field theory to quantum computation.[11,12]

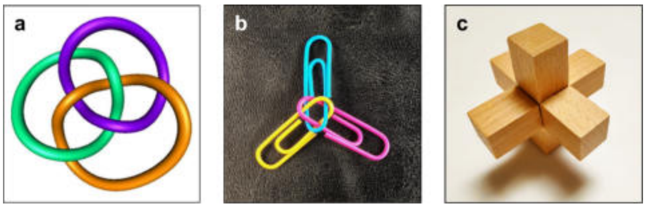

Figure 1. Examples of Borromean rings. (a) Three tubular loops interlinked in space. (b) Borromean linkage of paper clips. (c) Wooden Luban lock. As evidenced by the 3D arrangement of the paper clips, the three-component system cannot be laid flat in space; similarly, the Borromean rings cannot be made by interlacing three planar rigid rings in space.

The recent realization of topologically complex textures in structured light has shown great potential for technological applications.[13,14] Work on toroidal electromagnetic fields[15−17] developed to produce Möbius strips[18,19] and a zoo of topologies of increasing complexity, from torus knots, Hopf links, and knotted strips[20−23] to nested configurations of high-order topology.[24,25] Such structures have also emerged in nonlinear and incoherent light fields.[26,27] These developments ramified in the production of optical skyrmionic and hopfionic textures of various orders of complexity.[28−32] Concepts and methods of knot theory have facilitated the rapid growth and

Received: December 23, 2025
Revised: February 25, 2026
Accepted: February 25, 2026
Published: March 6, 2026

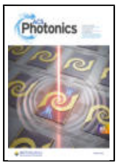

https://doi.org/10.1021/acsphotonics.5c03091
ACS Photonics 2026, 13, 1727−1733

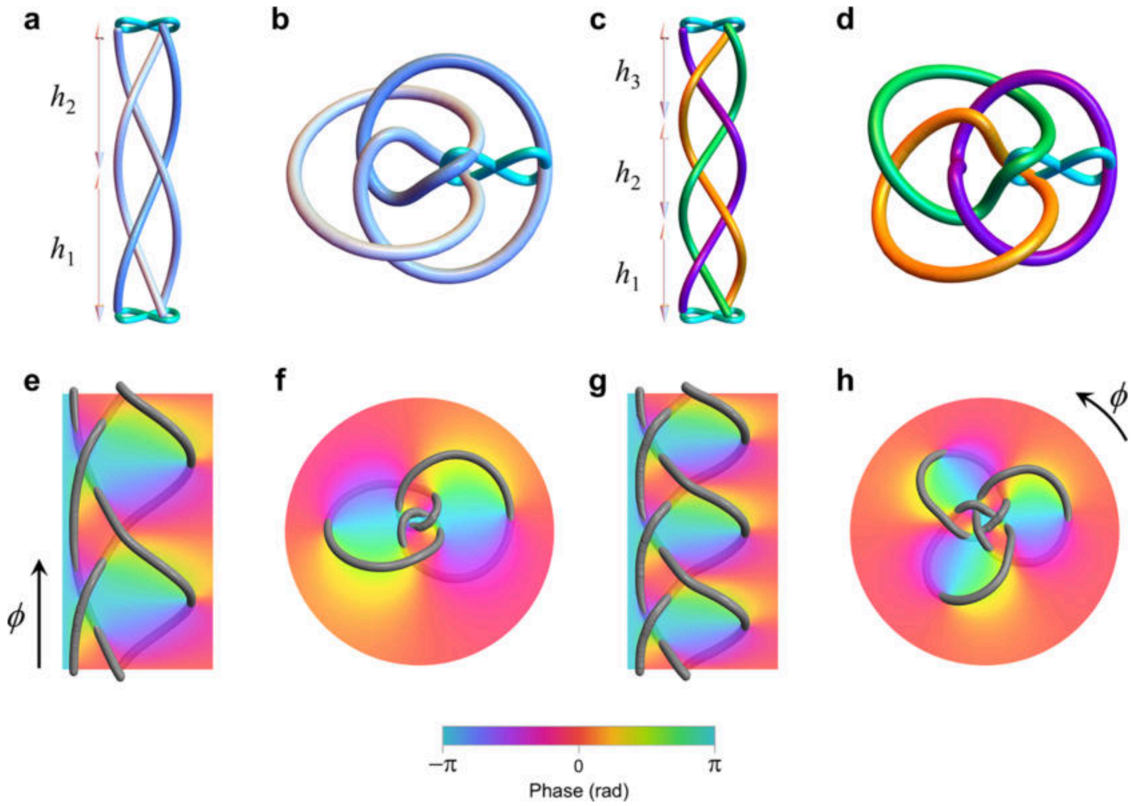

Figure 2. Construction of the figure-eight knot and Borromean rings by braided patterns. (a, c) Braid representation of the figure-eight knot and the Borromean rings displayed along the vertical axis. Note that both representations admit a projection onto the transverse plane of the braid given by a lemniscate curve (shown in cyan). The braid construction is prescribed by eq 2 with azimuthal strand separation given by $2\pi/3$ and h_n ($n = 1, 2, 3$) denoting the fundamental braid unit. (b, d) The standard representation of the figure-eight knot and Borromean rings prescribed by eq 1 with $a = 1.5$, $b = 1$, and $q = 2$. (e, g) Braided vortex lines relative to the mathematical braids shown in (a) and (c); the complex zeros are shown with their phase profile, with azimuthal angle ϕ ranging between $-\pi$ and π. (f, h) Figure-eight vortex knot and Borromean vortex rings with corresponding phase profile at $z = 0$.

creation of optical topological textures.[33−35] Promising applications are envisaged in optical metrology,[36] optical encoding,[22,24] and quantum information.[37,38] However, the demonstration of propagating coherent light in free space forming Borromean rings has remained so far elusive.

In this paper, we show how to experimentally create a set of optical Borromean vortex rings by using monochromatic structured light fields. We derive an explicit expression for the Borromean vortex rings and the generalized figure-eight vortex knot family from the topologically equivalent braided zeros of the wave function. In contrast to the pairwise linked rings in a Hopf vortex link, any two components of the optical Borromean vortex rings are unlinked. The topological control of the Borromean vortex rings relies on the accurate adjustment of zeros in a complex space. Using complex amplitude modulation, we generate the Borromean vortex rings experimentally, and by digital holographic measurements, we verify the topological properties of the system. Our findings represent a significant advance in the design and realization of complex light field textures, providing new grounds for studying their dynamical properties for future applications.

■ RESULTS

Mathematical Construction

In knot theory, every knot or link can be deformed to take the shape of a closed braid obtained by rearranging the system in a toroidal shape. The closed braid is then conveniently studied by the alternative representation given by virtually cutting open the braid along an azimuthal plane and by rearranging the system along a vertical axis. This sequence of transformations is performed by preserving the original strand orientation, crossing type, and topology. The mathematical construction of the Borromean vortex rings follows this strategy. The three space curves that trace out the Borromean rings are given by the following parametric equations:

$$\mathbf{r}_j(s, n) = \{x_j(s, n), y_j(s, n), z_j(s, n)\} = \begin{Bmatrix} [a + b\cos(ns + 2j\pi)/3]\cos(s), \\ [a + b\cos(ns + 2j\pi)/3]\sin(s), \\ \sin[2(ns + 2j\pi)/3]/q \end{Bmatrix} \tag{1}$$

where $\mathbf{r}_j$ denotes the vector position of the jth loop ($j = 1, 2, 3$) in space, $s \in [0, 2\pi)$ is the position of a point on each $\mathbf{r}_j$, and n is the winding number (a topological invariant quantity) that determines the topological configuration of the system, and a, b, and q are configuration parameters that determine the relative spacing of the three curves. To understand the final construction, let us consider first the braid representation of the figure-eight knot. As illustrated in Figure 2a, the straight braid representation is displayed along the vertical axis. By joining the corresponding end points, its closure gives the standard figure-eight knot shown in Figure 2b. Here the contribution of the three strands in the braid is visualized by

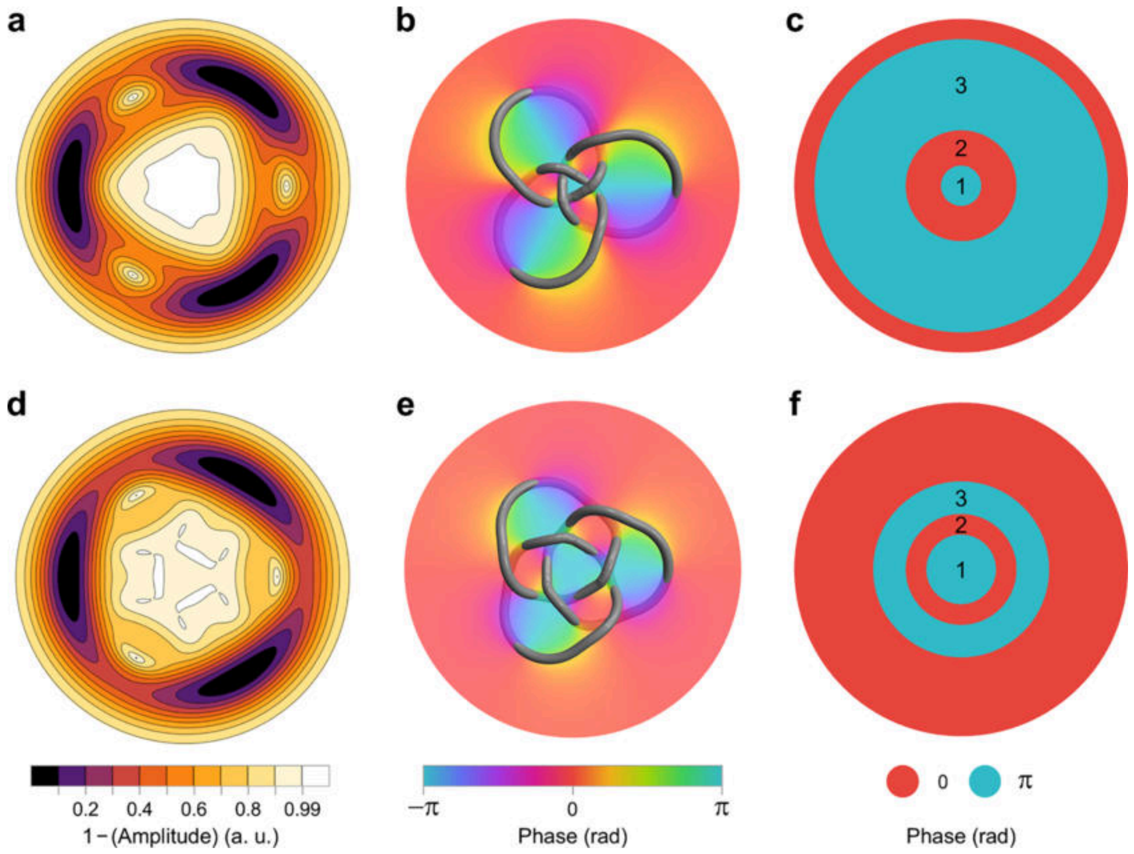

Figure 3. Amplitude and phase information on a topologically adjusted optical Borromean vortex rings. (a) The unmodified amplitude profile of the Borromean vortex rings with Gaussian waist $w_3 = 1$ and configuration parameter $\varepsilon = 1$. (b) Unmodified 2D phase profile and 3D topological structure of the Borromean vortex rings. (c) The relative spacing of the three vortex rings for $\varepsilon = 1$. (d) The adjusted amplitude profile for $w_3 = 0.67$ and $\varepsilon = 3$, where the location of all of the phase singularities is clearly visible. (e) The modified phase profile with the corresponding Borromean vortex rings. (f) The relative spacing of the three vortex rings for $\varepsilon = 3$.

different shades of blue. The braid patterns are composed by two identical subpatterns denoted by h_1 and h_2 representing the fundamental braid units. Topology is encapsulated by the relative winding of the three strands ($n = 2$), given by the sequence of the apparent crossings between each pair of strands. If we think of the strands as particle trajectories, their projection onto the transverse plane determines a lemniscate curve (shown in cyan). It is worth noting that this projection trajectory determines the figure-eight knot family, which is fundamentally different from the circular trajectory formed by the torus vortex knot. The geometric construction of the topological arrangement of the knot as a braid can be applied similarly to the Borromean rings and its braid, as shown in Figure 2c,d, where $n = 3$, $a = 1.5$, $b = 1$, and $q = 2$.

Interpreting the braid strands as zeros of a 3D complex scalar field $B = B_n(u, h)$, where u is a complex variable and $h \in [0, 2\pi]$ is a height parameter, we can proceed to the construction of the braided zeros of the optical Borromean vortex rings in a complex space.[20,39] This is done by taking

$$B_n(u, h) = \prod_{j=1}^{3} (u - \{\cos[(nh + 2j\pi)/3] + i\sin[2(nh + 2j\pi)/3]/2\}) \tag{2}$$

where the zeros that form the braid are placed in the complex plane u at different heights h. The braided vortex lines with phase profiles are shown in Figure 2e,g. By reverting the construction above, we obtain the vortex lines and phase profiles of the standard figure-eight knot and Borromean rings. This is done by mapping the height function to exponential function $v = \exp(ih)$ (i is the imaginary unit). Equation 2 becomes

$$\begin{aligned} C_n(u, v, \varepsilon) = {} & \varepsilon 64u^3 - 12u(3 + 2v^n - 2v^{*n}) - v^{2n} + v^{*2n} \\ & - 14(v^n + v^{*n}) \end{aligned} \tag{3}$$

where v^* is the complex conjugate of v. It is important to note the addition of configuration parameter ε in eq 3, which enables direct adjustment of the topologies within the complex space. The case of $\varepsilon = 1$ gives the unmodified complex polynomial.

The Borromean vortex rings are generated by the zeros of complex function $C_n(u, v, \varepsilon)$ for $n = 3$. Since both u and v are complex variables, the complex function can be regarded as a function in 4D real space.[40] The standard 3D Borromean vortex rings are then obtained by mapping the zeros of the complex function onto its stereographic projection.[41] In cylindrical coordinates (R, ϕ, z), the complex fields of the figure-eight knot and Borromean rings at $z = 0$, shown respectively in Figure 2f,h, are given by

$$\begin{aligned} f_n(R, \phi, 0, \varepsilon) = {} & \varepsilon 16(R^2 - 1)^3(R^2 + 1)^{2n-3} - 3(R^2 - 1)(R^2 + 1)^{n-1} \\ & \times [-2^{n+1}R^n e^{-in\phi} + 2^{n+1}R^n e^{in\phi} + 3(R^2 + 1)^n] + 4^{n-1}R^{2n}e^{-i2n\phi} \\ & - 4^{n-1}R^{2n}e^{i2n\phi} - 7 \times 2^{n-1}R^n e^{-in\phi}(1 + e^{i2n\phi})(1 + R^2)^n \end{aligned} \tag{4}$$

https://doi.org/10.1021/acsphotonics.5c03091

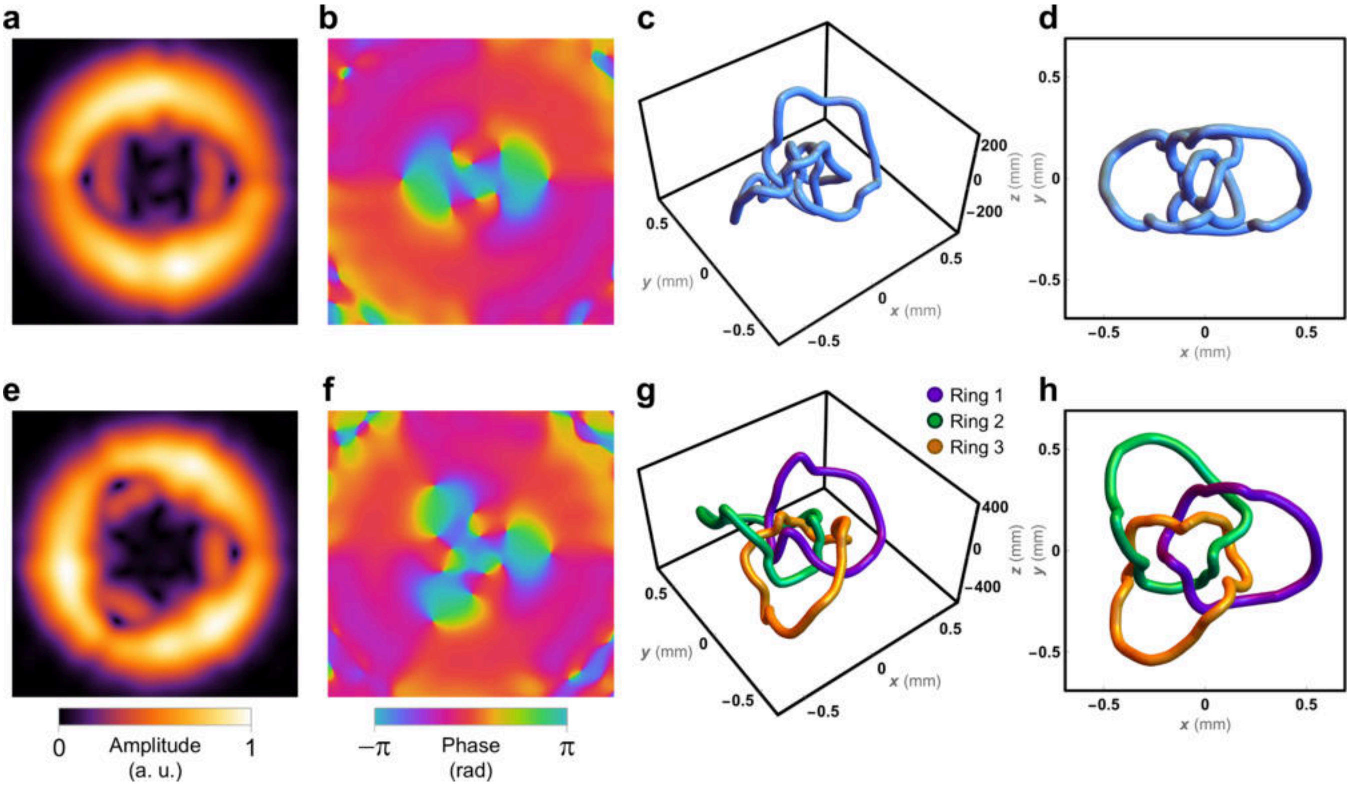

Figure 4. Measured light fields and reconstructed topology of the figure-eight vortex knot (top) and the Borromean vortex rings (bottom). (a, e) Measured amplitude and (b, f) phase profiles at $z = 0$. The corresponding 3D singularity structures are obtained by topological reconstruction and are shown from different viewing angles in (c, g) and (d, h), where the Borromean vortex rings are visualized in different colors. The achieved target topological structure can be checked by the relative crossings.

The derivation of the complex function $f_n(R, \phi, z)$ is provided (see Note 1 in the Supporting Information for details).

Topological Adjustment of Optical Borromean Vortex Rings

The complex polynomial $f_n(R, \phi, z)$ provides the explicit expression for the 3D Borromean vortex rings as well as the figure-eight vortex knot family. To produce an effective solution in a monochromatic light field, we need to modify the topological complex field given by eq 4 in real and complex space. In addition to the specific phase distribution, control of the amplitude distribution of the complex field is also quite important for the stability of the Borromean vortex rings. Since the amplitude of the polynomial $f_n(R, \phi, 0, \varepsilon)$ grows exponentially with the spatial coordinate R, the effective information gets gradually lost with increasing R. In real space, better control can be attained by applying a Gaussian profile of waist w_n to compensate for the excessive amplitude growth. The light fields can thus be appropriately gauged by the modified function

$$F_n(R, \phi, 0, \varepsilon, w_n) = f_n(R, \phi, 0, \varepsilon)\exp(-R^2/2{w_n}^2) \tag{5}$$

The adjustment is applicable for acoustic and optical vortex knots.[42] However, not all the vortex lines of Borromean vortex rings can be equally well distinguished by the amplitude distribution of $F_n(R, \phi, 0, \varepsilon, w_n)$ because there is no w_n equally applicable to all the vortex lines. For large values of w_n, the singularities distant from the origin of the coordinates can be clearly distinguished from the amplitude contours of $1 - |F_n(R, \phi, 0, \varepsilon, w_n)|$, but for small values of w_n, these singularities become blurred, preventing full control of the amplitudes on demand (see Note 2 in the Supporting Information for details). As a result, the distribution of phase singularities becomes uneven, causing a concentration of the 3D vortex lines at the beam center, as shown in Figure 3a. This in turn triggers the interaction between experimental perturbations and darkness, producing spontaneous reconnections of vortex lines and the destruction of the target topological structure.[43] The 3D topological structure with its phase profile at $z = 0$ is shown in Figure 3b.

Since the Gaussian adjustment has no effect on the phase distribution of the light field, the phase structure is solely determined by the complex function $C_n(u, v, \varepsilon)$. Hence, any change of the light field can be mapped onto the modification of the complex functions. To understand how to modify this function, let us consider the physical role of complex functions u and v: these variables determine the geometry of a leading vortex ring with radius r_0 and a propagating vortex line. The polynomials in $C_n(u, v, \varepsilon)$ serve to generate various topologies.[17] The polynomial $64u^3 - 36u$, in particular, generates three distinct vortex rings with different radii, the toroidal singularities of which provide the reference locations where the Borromean rings lie. One such singularity has a radius r_0, while the other two are determined by the coefficients of this polynomial and r_0. The configuration factor ε introduced in eq 3 and present also in eq 4 serves to control the radius of the leading vortex ring. The relative spacing of the three vortex rings given by $\varepsilon = 1$ is shown in Figure 3c, where the radius of the second ring is r_0. By increasing ε, the radius of the third ring gets reduced, and the radius of the first ring increased; the case $\varepsilon = 3$ is shown in Figure 3f. By varying the Gaussian waist w_n and the configuration parameter ε, we can control and fine-tune the individual singularities against the amplitude contours and the vortex line topology, as shown in Figure 3d,e.

Experimental Observation of Optical Borromean Vortex Rings

The experimental scheme to generate the optical Borromean vortex rings is based on the use of a liquid crystal spatial light modulator (SLM) to artificially control the 2D complex amplitude distribution of the paraxial light wave. This way, we can observe a stable topological structure by the light propagation in free space. At $z = 0$, the profiles generated by $F_n(R, \phi, 0, \varepsilon, w_n)$ have the same distribution as those of the polynomials that satisfy the paraxial wave equation, thus providing a perfect condition to modulate the light field to match the complex amplitude profiles of F_n in the experiment. This condition is validated by the Laguerre−Gaussian mode decomposition of F_n by the set of orthogonal modes $\mathrm{LG}_{l,p}$ with azimuthal index l and radial index p.

Compared with the production of vortex torus knots,[44] the mode decomposition of the figure-eight vortex knot and Borromean vortex rings is certainly more elaborate and challenging, with modes of opposite topological charge given by the simultaneous presence of v and v^* in eq 3. Here we should stress that the Gaussian waist w_n plays a different role from that of the LG modes: waist w_n governs the mode coefficient that forms the optical Borromean vortex rings, whereas the LG mode waist controls the size of the beam. The waist value for the optical figure-eight knot is $w_2 = 0.85$, and that for the Borromean rings is $w_3 = 0.67$. The derivation of the LG mode decomposition is provided (see Note 3 in the Supporting Information for details). The calculated mode coefficients are sufficient for the experiment without requiring further iterative optimization.

The incident laser beam (of wavelength $\lambda = 632.8$ nm) is modulated by SLM loading a phase-only pattern that encodes the amplitude and the phase distribution of the topological light field.[45] The SLM is then imaged by a 4f system consisting of two lenses, and the desired topological light field is injected into the first-order diffracted component. To observe the singularity structure of the optical Borromean vortex rings, we employed a single-shot method based on digital holography and the use of a CCD camera to record the digital interference field.[46,47] From the recorded hologram, we obtain the amplitude and phase distributions of the desired topological light field at $z = 0$, as shown in Figure 4a,b,e,f. The 3D full-field reconstruction is obtained from the information on angular spectrum transmission, and the 3D singularity structure is extracted from the intersection of the zero-value surfaces of the real and imaginary parts of the complex scalar field. The figure-eight vortex knot and the Borromean vortex rings were analyzed within 3D volumes corresponding to propagation distances of 500 and 900 mm, respectively. The experimental results of the figure-eight vortex knot are presented in Figure 4c,d. The generated Borromean vortex rings are rendered in different colors, as shown in Figure 4g,h. The strand crossings provide evidence of the achieved target topological structure. More details of the experiment and topological reconstruction are provided (see Note 4 in the Supporting Information and Methods).

CONCLUSIONS

We have demonstrated the actual production of an optical figure-eight vortex knot and the more challenging generation of optical Borromean vortex rings by using SLM-based methods. Other optical methods based on recently developed metasurfaces can also generate topologically complex light fields,[24] and the spatial scale of the realized structures is greatly reduced.[48] Furthermore, the artificial materials enable simultaneous control of the complex amplitude and polarization of light waves, thereby providing an integrated platform for the generation of a polarized topology.[21,22,49] The strategy of synthesizing Borromean rings by using independent toroidal vortex wave fields turns out to be ineffective within monochromatic laser beams (see Note 5 in the Supporting Information for details). By employing specially designed metasurfaces, Borromean vortex rings are expected to be realized in multiwavelength light fields.[24]

We proposed a noniterative strategy for adjusting the topological structure in complex space, which offers an effective approach for the rapid design of vortex topologies. By combining the modified stereographic projection, each component of the Borromean vortex rings is expected to be sculpted on demand.[50] As we saw, the design of topologically complex light field structures relies on the understanding and use of several techniques from knot theory, high-dimensional complex analysis, and appropriate mappings. As the topology of the system becomes more complex, the number of phase singularities in the light field is expected to increase, and this will pose greater difficulty in the overall control of the vortex topology. A combination of improved technology and artificial intelligence assisted analysis will surely help to overcome these difficulties.[51]

Other aspects related to the topological and dynamical stabilities of the target structures are also important. Recent results obtained from the numerical evolution of Borromean vortex rings in condensed matter physics have shown that those defects quickly reconnect to produce unknotted and unlinked loops through a rapid topological degradation of the initial system.[6] Similar mechanisms are expected to occur for light field structures. At this moment in time, the topological stability of the optical Borromean rings represents an open and interesting problem worth investigating, where the exploration and comparison of features related to the reconnection of light fields play a fundamental role in the process. All of this is quite challenging but will no doubt be important for future applications in light−matter interactions and information encoding technology.

METHODS

Reconstruction of the 3D Vortex Structures

Data extracted from the complex amplitude profiles and angular spectrum information obtained from the propagating volume are used to reconstruct the topology of the vortex lines. The data set is based on 101 profiles equispaced along the z-axis, from which we compute the zero isosurfaces of the real and imaginary parts of the 3D complex scalar field. This is done by creating a discrete surface triangulation and then applying a surface intersection extraction algorithm developed in-house to reconstruct the singular trajectories of the vortex lines. This method proves to be fast and highly accurate.

■ ASSOCIATED CONTENT

Data Availability Statement

Data underlying the results presented in this paper are not publicly available at this time but may be obtained from the authors upon reasonable request.

Supporting Information

The Supporting Information is available free of charge at https://pubs.acs.org/doi/10.1021/acsphotonics.5c03091.

Details about the derivation of the complex polynomial and mode decomposition, the experimental setup, and the topological adjustment strategy (PDF)

■ AUTHOR INFORMATION

Corresponding Author

Qiwen Zhan − *School of Optical-Electrical and Computer Engineering, University of Shanghai for Science and Technology, Shanghai 200093, China; Zhangjiang Laboratory, Shanghai 201204, China; Zhejiang Key Laboratory of 3D Micro/Nano Fabrication and Characterization, Department of Electronic and Information Engineering, School of Engineering, Westlake University, Hangzhou 310030 Zhejiang, China; Westlake Institute for Optoelectronics, Hangzhou 311421, China; International Institute for Sustainability with Knotted Chiral Meta Matter (WPI-SKCM^2), Hiroshima University, Higashihiroshima, Hiroshima 739-8526, Japan*; Email: qwzhan@usst.edu.cn

Authors

Jinzhan Zhong − *School of Optical-Electrical and Computer Engineering, University of Shanghai for Science and Technology, Shanghai 200093, China; Zhangjiang Laboratory, Shanghai 201204, China*; orcid.org/0000-0002-2438-7911

Renzo L. Ricca − *Department of Mathematics and Applications, University of Milano-Bicocca, 20125 Milano, Italy; Faculty of Science, Beijing U. Technology, Beijing 100124, China; International Institute for Sustainability with Knotted Chiral Meta Matter (WPI-SKCM^2), Hiroshima University, Higashihiroshima, Hiroshima 739-8526, Japan*

Complete contact information is available at: https://pubs.acs.org/10.1021/acsphotonics.5c03091

Author Contributions

Q.Z. and R.L.R. proposed the project. Q.Z. supervised the project. J.Z. implemented the theory and performed the experiments. All authors contributed equally to write the paper.

Notes

The authors declare no competing financial interest.

■ ACKNOWLEDGMENTS

J.Z. and Q.Z. acknowledge financial support from the National Key R&D Program of China (2025YFF0515101), the National Natural Science Foundation of China (NSFC) (12434012, 12304367, and 62535013), the Shanghai Rising-Star Program (23YF1415800), and the Shanghai Postdoctoral Excellence Program (2023533). Q.Z. and R.L.R. wish to acknowledge the kind hospitality of the International Institute for Sustainability with Knotted Chiral Meta Matter (WPI-SKCM^2) of Hiroshima University, where part of this work originated.

■ REFERENCES

(1) Adams, C. C. *The knot book*; American Mathematical Society, 2004.

(2) Ricca, R. L.; Nipoti, B. Gauss' Linking Number Revisited. *J. Knot Theor. Ramif.* **2011**, *20* (10), 1325−1343.

(3) Ruzmaikin, A.; Akhmetiev, P. Topological invariants of magnetic fields, and the effect of reconnections. *Phys. Plasmas* **1994**, *1* (2), 331−336.

(4) Tkalec, U.; Ravnik, M.; Čopar, S.; Žumer, S.; Muševič, I. Reconfigurable knots and links in chiral nematic colloids. *Science* **2011**, *333* (6038), 62−65.

(5) Yang, W.-C.; Tsubota, M.; Nitta, M.; Zeng, H.-B. Macroscopic Borromean and anti-Borromean states of quantized vortices. *Phys. Rev. A* **2025**, *111* (2), No. 023319.

(6) Guan, H.; Zuccher, S.; Liu, X. Topological cascade of quantum Borromean rings. *Phys. Fluids* **2025**, *37* (2), No. 024126.

(7) Mao, C.; Sun, W.; Seeman, N. C. Assembly of Borromean rings from DNA. *Nature* **1997**, *386* (6621), 137−138.

(8) Chichak, K. S.; Cantrill, S. J.; Pease, A. R.; Chiu, S.-H.; Cave, G. W. V.; Atwood, J. L.; Stoddart, J. F. Molecular Borromean Rings. *Science* **2004**, *304* (5675), 1308−1312.

(9) Thorp-Greenwood, F. L.; Kulak, A. N.; Hardie, M. J. An infinite chainmail of M6L6 metallacycles featuring multiple Borromean links. *Nat. Chem.* **2015**, *7* (6), 526−531.

(10) Zhang, H.-N.; Jin, G.-X. Synthesis of molecular Borromean links featuring trimeric metallocages. *Nat. Synth.* **2025**, *4* (4), 488−496.

(11) Chan, A. P. O.; Ye, P.; Ryu, S. Braiding with Borromean Rings in (3 + 1)-Dimensional Spacetime. *Phys. Rev. Lett.* **2018**, *121* (6), No. 061601.

(12) Iqbal, M.; Tantivasadakarn, N.; Verresen, R.; Campbell, S. L.; Dreiling, J. M.; Figgatt, C.; Gaebler, J. P.; Johansen, J.; Mills, M.; Moses, S. A.; Pino, J. M.; Ransford, A.; Rowe, M.; Siegfried, P.; Stutz, R. P.; Foss-Feig, M.; Vishwanath, A.; Dreyer, H. Non-Abelian topological order and anyons on a trapped-ion processor. *Nature* **2024**, *626* (7999), 505−511.

(13) Forbes, A.; de Oliveira, M.; Dennis, M. R. Structured light. *Nat. Photonics* **2021**, *15* (4), 253−262.

(14) He, C.; Shen, Y.; Forbes, A. Towards higher-dimensional structured light. *Light Sci. Appl.* **2022**, *11*, 205.

(15) Wan, C.; Cao, Q.; Chen, J.; Chong, A.; Zhan, Q. Toroidal vortices of light. *Nat. Photonics* **2022**, *16* (7), 519−522.

(16) Zdagkas, A.; McDonnell, C.; Deng, J.; Shen, Y.; Li, G.; Ellenbogen, T.; Papasimakis, N.; Zheludev, N. I. Observation of toroidal pulses of light. *Nat. Photonics* **2022**, *16* (7), 523−528.

(17) Zhong, J.; Teng, H.; Zhan, Q. Toroidal phase topologies within paraxial laser beams. *Commun. Phys.* **2024**, *7* (1), 285.

(18) Zhong, J.; Wan, C.; Zhan, Q. Optical Twisted Phase Strips. *ACS Photonics* **2023**, *10* (9), 3384−3389.

(19) Bauer, T.; Banzer, P.; Karimi, E.; Orlov, S.; Rubano, A.; Marrucci, L.; Santamato, E.; Boyd, R. W.; Leuchs, G. Observation of optical polarization Möbius strips. *Science* **2015**, *347* (6225), 964−966.

(20) Dennis, M. R.; King, R. P.; Jack, B.; O'Holleran, K.; Padgett, M. J. Isolated optical vortex knots. *Nat. Phys.* **2010**, *6* (2), 118−121.

(21) Larocque, H.; Sugic, D.; Mortimer, D.; Taylor, A. J.; Fickler, R.; Boyd, R. W.; Dennis, M. R.; Karimi, E. Reconstructing the topology of optical polarization knots. *Nat. Phys.* **2018**, *14* (11), 1079−1082.

(22) Larocque, H.; D'Errico, A.; Ferrer-Garcia, M. F.; Carmi, A.; Cohen, E.; Karimi, E. Optical framed knots as information carriers. *Nat. Commun.* **2020**, *11*, 5119.

(23) Zhong, J.; Liu, S.; Guo, X.; Li, P.; Wei, B.; Han, L.; Qi, S.; Zhao, J. Observation of optical vortex knots and links associated with topological charge. *Opt. Express* **2021**, *29* (23), 38849−38857.

(24) Kong, L.-J.; Zhang, W.; Li, P.; Guo, X.; Zhang, J.; Zhang, F.; Zhao, J.; Zhang, X. High capacity topological coding based on nested vortex knots and links. *Nat. Commun.* **2022**, *13*, 2705.

(25) Zhong, J.; Teng, H.; Zhan, Q. Generation of High-Order Optical Vortex Knots and Links. *ACS Photonics* **2025**, *12* (3), 1683−1688.

(26) Gao, J.; Barati Sedeh, H.; Tsvetkov, D.; Pires, D. G.; Vincenti, M. A.; Xu, Y.; Kravchenko, I.; George, R.; Scalora, M.; Feng, L.; Litchinitser, N. M. Topology-imprinting in nonlinear metasurfaces. *Sci. Adv.* **2025**, *11* (24), No. eadv5190.

(27) Wang, Z.; Lu, X.; Chen, Z.; Cai, Y.; Zhao, C. Topological links and knots of speckled light mediated by coherence singularities. *Light Sci. Appl.* **2025**, *14* (1), 175.

(28) Sugic, D.; Droop, R.; Otte, E.; Ehrmanntraut, D.; Nori, F.; Ruostekoski, J.; Denz, C.; Dennis, M. R. Particle-like topologies in light. *Nat. Commun.* **2021**, *12*, 6785.

(29) Wan, C.; Shen, Y.; Chong, A.; Zhan, Q. Scalar optical hopfions. *eLight* **2022**, *2*, 22.

(30) Ehrmanntraut, D.; Droop, R.; Sugic, D.; Otte, E.; Dennis, M. R.; Denz, C. Optical second-order skyrmionic hopfion. *Optica* **2023**, *10* (6), 725−731.

(31) Mata-Cervera, N.; Sharma, D. K.; Shen, Y.; Paniagua-Dominguez, R.; Porras, M. A. Skyrmionic Polarization Texture around the Phase Singularity of Optical Vortices. *Phys. Rev. Lett.* **2025**, *135* (3), No. 033805.

(32) Irvine, W. T. M.; Bouwmeester, D. Linked and knotted beams of light. *Nat. Phys.* **2008**, *4* (9), 716.

(33) Zhan, Q. Spatiotemporal sculpturing of light: a tutorial. *Adv. Opt. Photon.* **2024**, *16* (2), 163−228.

(34) Shen, Y.; Zhang, Q.; Shi, P.; Du, L.; Yuan, X.; Zayats, A. V. Optical skyrmions and other topological quasiparticles of light. *Nat. Photonics* **2024**, *18* (1), 15−25.

(35) Dennis, M. R. Designing Knotted Fields in Light and Electromagnetism. *Knotted Fields*; Ricca, R. L., Liu, X., Eds.; Springer Nature, Cham, Switzerland, 2024; pp 181−242.

(36) Du, L.; Yang, A.; Zayats, A. V.; Yuan, X. Deep-subwavelength features of photonic skyrmions in a confined electromagnetic field with orbital angular momentum. *Nat. Phys.* **2019**, *15* (7), 650−654.

(37) Ornelas, P.; Nape, I.; de Mello Koch, R.; Forbes, A. Non-local skyrmions as topologically resilient quantum entangled states of light. *Nat. Photonics* **2024**, *18* (3), 258−266.

(38) Li, J.-K.; Sun, K.; Hao, Z.-Y.; Liang, J.-H.; Tao, S.-J.; Pachos, J. K.; Xu, J.-S.; Han, Y.-J.; Li, C.-F.; Guo, G.-C. Photonic Simulation of Majorana-Based Jones Polynomials. *Phys. Rev. Lett.* **2024**, *133* (23), No. 230603.

(39) King, R. P. Knotting of optical vortices. Ph.D. Thesis, University of Southampton, 2010.

(40) *Knotted fields*; Ricca, R. L., Liu, X., Eds.; Lecture Notes in Mathematics, Vol. *2344*; Springer Nature, 2024.

(41) Sutcliffe, P. M.; Winfree, A. T. Stability of knots in excitable media. *Phys. Rev. E* **2003**, *68* (1), No. 016218.

(42) Zhang, H.; Zhang, W.; Liao, Y.; Zhou, X.; Li, J.; Hu, G.; Zhang, X. Creation of acoustic vortex knots. *Nat. Commun.* **2020**, *11*, 3956.

(43) Padgett, M. J.; O'Holleran, K.; King, R. P.; Dennis, M. R. Knotted and tangled threads of darkness in light beams. *Contemp. Phys.* **2011**, *52* (4), 265−279.

(44) Leach, J.; Dennis, M. R.; Courtial, J.; Padgett, M. J. Laser beams: knotted threads of darkness. *Nature* **2004**, *432* (7014), 165.

(45) Bolduc, E.; Bent, N.; Santamato, E.; Karimi, E.; Boyd, R. W. Exact solution to simultaneous intensity and phase encryption with a single phase-only hologram. *Opt. Lett.* **2013**, *38* (18), 3546−3549.

(46) Zhong, J.; Liu, S.; Guo, X.; Li, P.; Wei, B.; Qi, S.; Zhao, J. Reconstructing the topology of optical vortex lines with single-shot measurement. *Appl. Phys. Lett.* **2021**, *119* (16), 161102.

(47) Pires, D. G.; Tsvetkov, D.; Barati Sedeh, H.; Chandra, N.; Litchinitser, N. M. Stability of optical knots in atmospheric turbulence. *Nat. Commun.* **2025**, *16* (1), 3001.

(48) Wang, L.; Zhang, W.; Yin, H.; Zhang, X. Ultrasmall Optical Vortex Knots Generated by Spin-Selective Metasurface Holograms. *Adv. Opt. Mater.* **2019**, *7* (10), No. 1900263.

(49) Guo, X.; Li, P.; Zhong, J.; Liu, S.; Wei, B.; Zhu, W.; Qi, S.; Cheng, H.; Zhao, J. Tying Polarization-Switchable Optical Vortex Knots and Links via Holographic All-Dielectric Metasurfaces. *Laser Photon. Rev.* **2020**, *14* (3), No. 1900366.

(50) Tsvetkov, D.; G Pires, D.; Barati Sedeh, H.; M Litchinitser, N. Sculpting isolated optical vortex knots on demand. *Photon. Res.* **2025**, *13* (2), 527−540.

(51) Wetzstein, G.; Ozcan, A.; Gigan, S.; Fan, S.; Englund, D.; Soljačić, M.; Denz, C.; Miller, D. A. B.; Psaltis, D. Inference in artificial intelligence with deep optics and photonics. *Nature* **2020**, *588* (7836), 39−47.

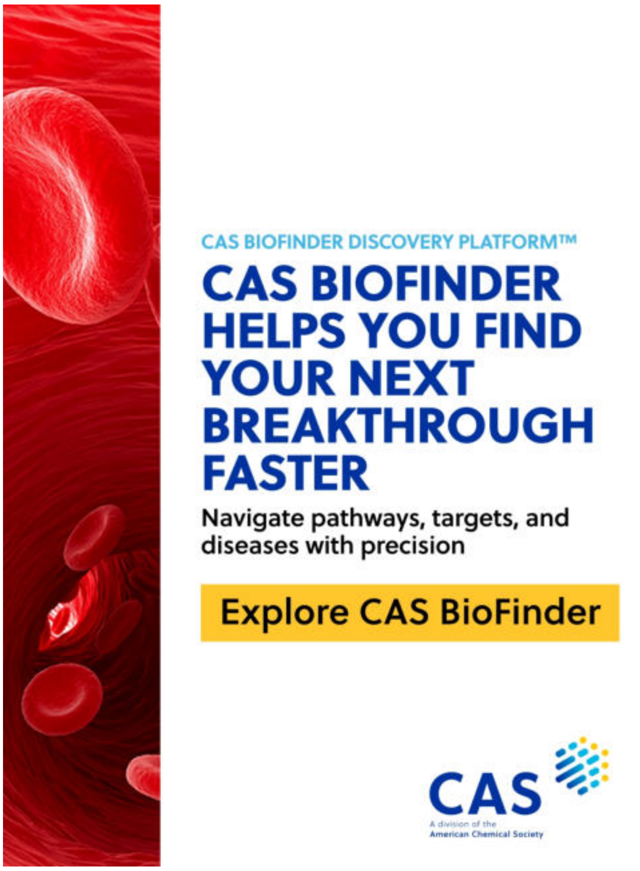

Supporting Information:

Optical Borromean Vortex Rings

Jinzhan Zhong[1,2], Renzo L. Ricca[3,4,7], Qiwen Zhan[1,2,5,6,7,*]

[1]School of Optical-Electrical and Computer Engineering, University of Shanghai for Science and Technology, Shanghai 200093, China

[2]Zhangjiang Laboratory, 100 Haike Road, Shanghai, 201204, China

[3]Department of Mathematics and Applications, University of Milano-Bicocca, Via Cozzi 55, 20125 Milano, Italy

[4]Faculty of Science, Beijing U. Technology, 100 Pingleyuan, Beijing 100124, China

[5]Zhejiang Key Laboratory of 3D Micro/Nano Fabrication and Characterization, Department of Electronic and Information Engineering, School of Engineering, Westlake University, Hangzhou, 310030, Zhejiang, China

[6]Westlake Institute for Optoelectronics, Fuyang, Hangzhou, 311421, China

[7]International Institute for Sustainability with Knotted Chiral Meta Matter (WPI-SKCM^2), Hiroshima University, Higashihiroshima, Hiroshima 739-8526, Japan

*Correspondence to: qwzhan@usst.edu.cn

Number of pages: 11

Number of figures: 3

Number of tables: 0

Note 1: Derivation of the complex polynomial of the figure-of-eight vortex knot family

The stereographic projection provides the mapping from the 2D complex space to the 3D real space. In cylindrical coordinates we define

$$\begin{aligned} u(R,\phi,z) &= \frac{R^2+z^2-1+2\mathrm{i}z}{R^2+z^2+1} \\ v(R,\phi,z) &= \frac{2R\mathrm{e}^{\mathrm{i}\phi}}{R^2+z^2+1} \\ v^*(R,\phi,z) &= \frac{2R\mathrm{e}^{-\mathrm{i}\phi}}{R^2+z^2+1} \end{aligned} \tag{S1}$$

The complex function u contains toroidal phase singularities in real space, while the complex function v and its conjucate function v^* represent the vortex and anti-vortex in real space. By mapping the complex function C of Eq. (3) to cylindrical coordinates, we get

$$Q_n\left[u(R,\phi,z),v(R,\phi,z),v^*(R,\phi,z)\right]=\frac{4}{\left(1+R^2+z^2\right)^{2n}}$$

$$\left\{\begin{aligned} &4^{n-1}R^{2n}e^{-i2n\phi}-4^{n-1}R^{2n}e^{i2n\phi}-7\times2^{n-1}R^ne^{-in\phi}\left(1+e^{i2n\phi}\right)\left(1+R^2+z^2\right)^n \\ &+16\left(1+R^2+z^2\right)^{2n-3}\left[R^2+(\mathrm{i}+z)^2\right]^3 \\ &-3\left[R^2+(\mathrm{i}+z)^2\right]\left(1+R^2+z^2\right)^{n-1}\left[-2^{n+1}R^ne^{-in\phi}+2^{n+1}R^ne^{in\phi}+3\left(1+R^2+z^2\right)^n\right] \end{aligned}\right\} \tag{S2}$$

The zero solutions of Q are given by considering the normalized numerator of the polynomial, this is given by

$$\begin{aligned} &f_n(R,\phi,z)=4^{n-1}R^{2n}e^{-i2n\phi}-4^{n-1}R^{2n}e^{i2n\phi} \\ &-7\times2^{n-1}R^ne^{-in\phi}\left(1+e^{i2n\phi}\right)\left(1+R^2+z^2\right)^n+16\left(1+R^2+z^2\right)^{2n-3}\left[R^2+(\mathrm{i}+z)^2\right]^3 \\ &-3\left[R^2+(\mathrm{i}+z)^2\right]\left(1+R^2+z^2\right)^{n-1}\left[-2^{n+1}R^ne^{-in\phi}+2^{n+1}R^ne^{in\phi}+3\left(1+R^2+z^2\right)^n\right] \end{aligned} \tag{S3}$$

This equation is further simplified by taking $z = 0$, we have

$$\begin{aligned} &f_n(R,\phi,0,\varepsilon)=4^{n-1}R^{2n}e^{-i2n\phi}-4^{n-1}R^{2n}e^{i2n\phi} \\ &-7\times2^{n-1}R^ne^{-in\phi}\left(1+e^{i2n\phi}\right)\left(1+R^2\right)^n+\varepsilon\cdot16\left(R^2-1\right)^3\left(R^2+1\right)^{2n-3} \\ &-3\left(R^2-1\right)\left(R^2+1\right)^{n-1}\left[-2^{n+1}R^ne^{-in\phi}+2^{n+1}R^ne^{in\phi}+3\left(R^2+1\right)^n\right] \end{aligned} \tag{S4}$$

The phase profiles of the polynomial f are shown in Figures 2f and 2h in main text, for $n = 2$ and $n = 3$.

Note 2: Change of amplitude due to a change in w_n

When w_n varies between 1 and 0.8, the singularities at larger R (in the outer ring region) are clearly distinguishable from the amplitude contours of $1-\left|F_n\left(R,\phi,0,\varepsilon,w_n\right)\right|$. As w_n decreases, the amplitudes around these singularities decrease as well, which results in a reduced definition of the contour lines. When w_n = 0.7 the other 6 singularities on the central ring region are still well defined, but the three singularities on the outer ring are blurred in the darkness, leaving the 3D singularity lines open. When the value of w_n is about 0.6 or 0.5, the three singularities on the outer ring can no longer be distinguished (even though the singularities in the central area remain distinguishable for w_n = 0.5, see Figure S1). Therefore, as far as the polynomial $F_n\left(R,\phi,0,\varepsilon,w_n\right)$ is concerned, the Gaussian adjustement with ε = 1 is ineffective in real space.

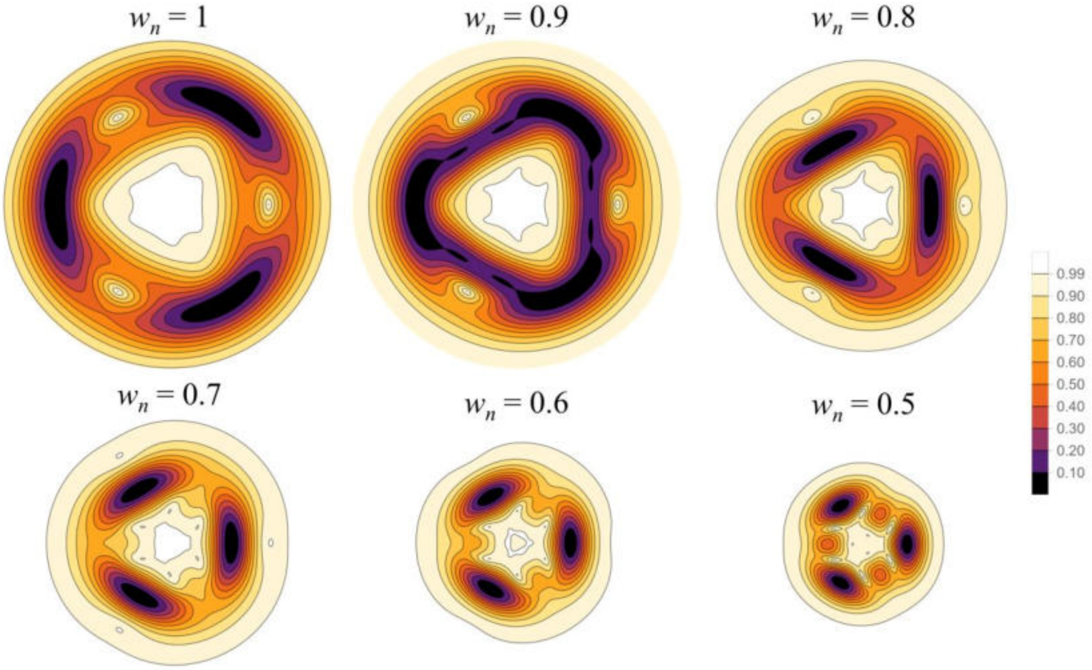

Figure S1. Amplitude contours for different values of w_n. The bright areas indicate low-amplitude values of F_n, and the tiny circles in the central areas of the bottom row insets represent the individual singularities.

Note 3: Derivation of the LG mode decomposition for the figure-of-eight vortex knot and the Borromean vortex rings

The topological light field can be expressed as a linear superposition of a series of LG modes, given by

$$\psi\left(R,\phi,w\right)=\sum c_{l,p}\mathrm{LG}_{l,p}\left(R,\phi,w\right) \tag{S5}$$

where $\mathrm{LG}_{l,p}$ denotes the Laguerre-Gaussian mode with azimuthal index l and radial index p, and ω the width of the mode. Here $\mathrm{LG}_{l,p}$ is defined by

$$\mathrm{LG}_{l,p}\left(R,\phi,w\right)=\sqrt{\frac{p!}{\pi\left(|l|+p\right)!}}\frac{1}{w^{|l|+1}}R^{|l|}e^{il\phi}e^{-\frac{R^2}{2w^2}}L_p^{|l|}\left(\frac{R^2}{w^2}\right) \tag{S6}$$

where $L|l|$ $p$is Laguerre’s polynomial and l represents the topological charge that can be either positive or negative[1]. For each mode, the corresponding coefficient is calculated by the following integral[2]

$$c_{l,p}\left(w\right)=\int_0^{2\pi}\int_0^{\infty}\mathrm{LG}_{-l,p}\left(R,\phi,w\right)f_n\left(R,\phi,0\right)\mathrm{LG}_{0,0}\left(R,\phi,w\right)RdRd\phi \tag{S7}$$

Explicit computations of the mode coefficients for the figure-of-eight vortex knot give:

$$\begin{aligned}
c_{0,0}&=3\left(-13+38w^2-228w^6+312w^8\right)\\
c_{0,1}&=6w^2\left(-19+342w^4-624w^6\right)\\
c_{0,2}&=108w^6\left(-19+52w^2\right)\\
c_{0,3}&=36w^6\left(19-104w^2\right)\\
c_{0,4}&=936w^8\\
c_{2,0}&=-2\sqrt{2}w^2\left(-5+42w^2+228w^4\right)\\
c_{2,1}&=4\sqrt{6}w^4\left(7+76w^2\right)\\
c_{2,2}&=-152\sqrt{3}w^6\\
c_{4,0}&=-8\sqrt{6}w^4\\
c_{-2,0}&=2\sqrt{2}w^2\left(-19-42w^2+60w^4\right)\\
c_{-2,1}&=4\sqrt{6}w^4\left(7-20w^2\right)\\
c_{-2,2}&=40\sqrt{3}w^6\\
c_{-4,0}&=8\sqrt{6}w^4
\end{aligned} \tag{S8}$$

To produce the optical figure-of-eight vortex knot experimentally we take $w = 0.85$. Explicit computations of the mode coefficients for the Borromean vortex rings give:

$$
\begin{aligned}
c_{0,0} &= 6\left(-\frac{13}{2}+6w^2+63w^4-756w^8-720w^{10}+4680w^{12}\right)\\
c_{0,1} &= -36w^2\left(1+3w^2\left(7+8w^4\left(-21-25w^2+195w^4\right)\right)\right)\\
c_{0,2} &= 54w^4\left(7-504w^4-800w^6+7800w^8\right)\\
c_{0,3} &= -864w^8\left(-21-50w^2+650w^4\right)\\
c_{0,4} &= 216w^8\left(-21+50w^2\left(-2+39w^2\right)\right)\\
c_{0,5} &= -4320w^{10}\left(-1+39w^2\right)\\
c_{0,6} &= 28080w^{12}\\
c_{3,0} &= -4\sqrt{6}w^3\left(-5+36w^2+660w^4+2280w^6\right)\\
c_{3,1} &= 24\sqrt{6}w^5\left(3+110w^2+570w^4\right)\\
c_{3,2} &= -48\sqrt{15}w^7\left(11+114w^2\right)\\
c_{3,3} &= 912\sqrt{30}w^9\\
c_{6,0} &= -192\sqrt{5}w^6\\
c_{-3,0} &= -4\sqrt{6}w^3\left(-19-132w^2-180w^4+600w^6\right)\\
c_{-3,1} &= -24\sqrt{6}w^5\left(-11-30w^2+150w^4\right)\\
c_{-3,2} &= 144\sqrt{15}w^7\left(-1+10w^2\right)\\
c_{-3,3} &= -240\sqrt{30}w^9\\
c_{-6,0} &= 192\sqrt{5}w^6
\end{aligned}
\tag{S9}
$$

To produce the optical Borromean vortex rings experimentally we take $w = 0.67$.

Note 4: On the experimental production and observation of the optical Borromean vortex rings

The experimental setup to generate and observe the optical Borromean vortex rings is shown in Figure S2a. The input laser beam is divided into two streams by a beam splitter (BS_1). The generative stream is modulated by a phase-type SLM, which controls the amplitude and phase distribution of the beam. The modulated light beam is then imaged by a $4f$ system consisting of two lenses L_1 and L_2 and an aperture, the latter being placed on a focal plane to obtain the required first order diffracted component. The target optical Borromean vortex rings are produced after the second lens L_2. To observe the 3D topological structure of the Borromean rings, the two split streams are recombined by a beam splitter BS_2, and the interference field is recorded by a CCD camera. The experimentally recorded hologram for the optical Borromean vortex rings is shown in Figure S2b. During the reconstruction process, appropriate spatial filtering can eliminate experimental noise without altering the topological structure. The reconstructed light field and the 3D topological structure of the optical Borromean vortex rings are shown in Fig. 4 in main text. The relative position of the Borromean vortex rings in space is provided by the three insets of Figure S2c that help to inspect and analze the details of the topology of the system in addition to the full overview provided by Figs. 4g and 4h in main text. From direct inspection of Figure S2c we can clearly see that any pair of rings results unlinked, while accurate inspection of the crossings in Figures 4g and 4h in main text ensures that the target topology is actually achieved.

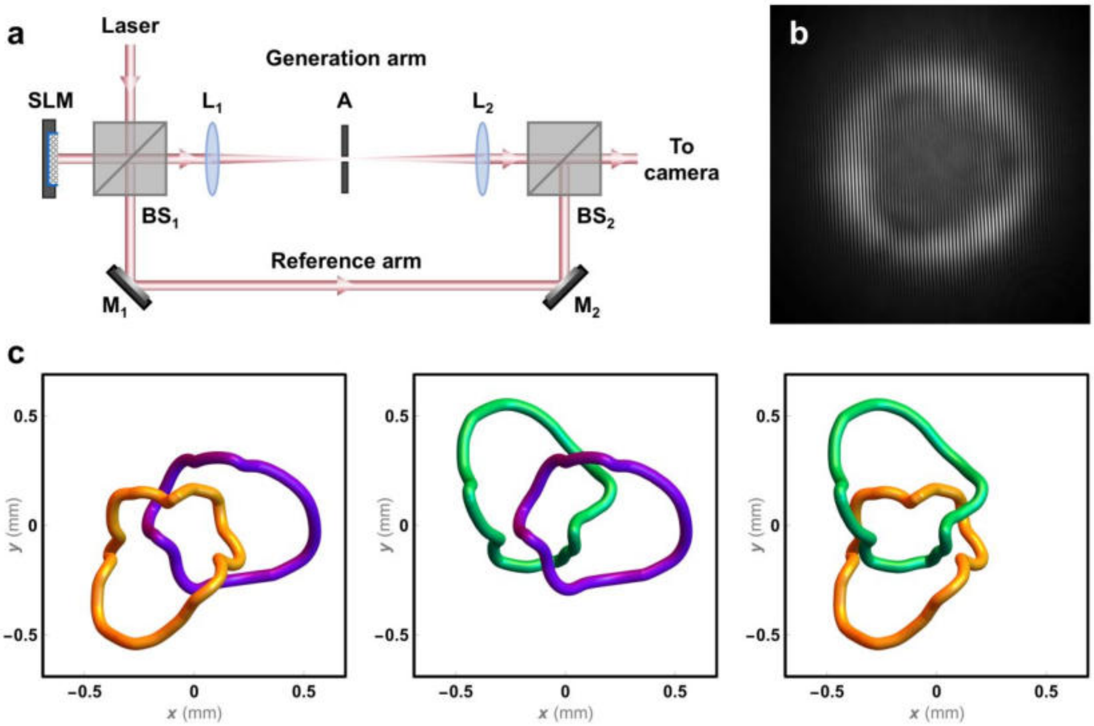

Figure S2. Experimental production and observation of optical Borromean vortex ring. (a) Experimental setup for the generation and measurement of the light field topology. SLM: spatial light modulator; BS_1, BS_2: beam splitters; L_1, L_2: lenses, A: aperture; M_1, M_2: mirrors. (b) Experimentally recorded hologram of the optical Borromean vortex rings. (c) Relative position of each pair of vortex rings extracted from the 3D system of optical Borromean vortex rings.

Note 5: Other possible strategy for constructing optical Borromean vortex rings

Mathematically, the Borromean rings can be defined by the following three parametric equations:

$$\begin{cases} \left[\cos\alpha, \sin\alpha+\sqrt{3}/3, \cos(3\alpha)/2\right] \\ \left[\cos\alpha+0.5, \sin\alpha-\sqrt{3}/6, \cos(3\alpha)/2\right] \\ \left[\cos\alpha-0.5, \sin\alpha-\sqrt{3}/6, \cos(3\alpha)/2\right] \end{cases} \tag{S10}$$

where $\alpha\in[0, 2\pi]$. Figure S3a shows the 3D structure of the Borromean rings in different perspective views. In this configuration, the Borromean rings are composed of three identical loops arranged at distinct spatial locations. In monochromatic structured light, isolated vortex ring with the same topological configuration can be constructed by using LG modes[3]. For a single vortex ring, the topological light field can be expressed as

$$\psi = \mathrm{LG}_{0,0} - 4\mathrm{LG}_{0,1} + 0.8\mathrm{LG}_{3,0} \tag{S11}$$

The amplitude and phase distributions of the light field after shifting along the negative x-axis are shown in Figures 3b$_1$ and 3c$_1$, respectively. Since vortex topologies are defined by the zeros of 3D light field, in principle, three vortex rings can be generated by multiplying light fields that correspond to distinct spatial positions. For simplicity, we will only illustrate with two components. These two components are set to be shifted along the negative and positive x-axis, respectively, each forming an isolated vortex ring within a distinct beam. The amplitude and phase distributions of the product of the two fields are shown in Figures 3b$_3$ and c$_3$. While the phase singularities of both fields are retained at z=0 plane, they cannot evolve into two separate vortex rings in the 3D space. The changes in amplitude and phase distributions across the overlap region lead to the formation of tangled singularity lines in 3D space. Although this strategy is ineffective for monochromatic light, it is expected to be implemented by mapping three vortex loops to multi-wavelength beams[4].

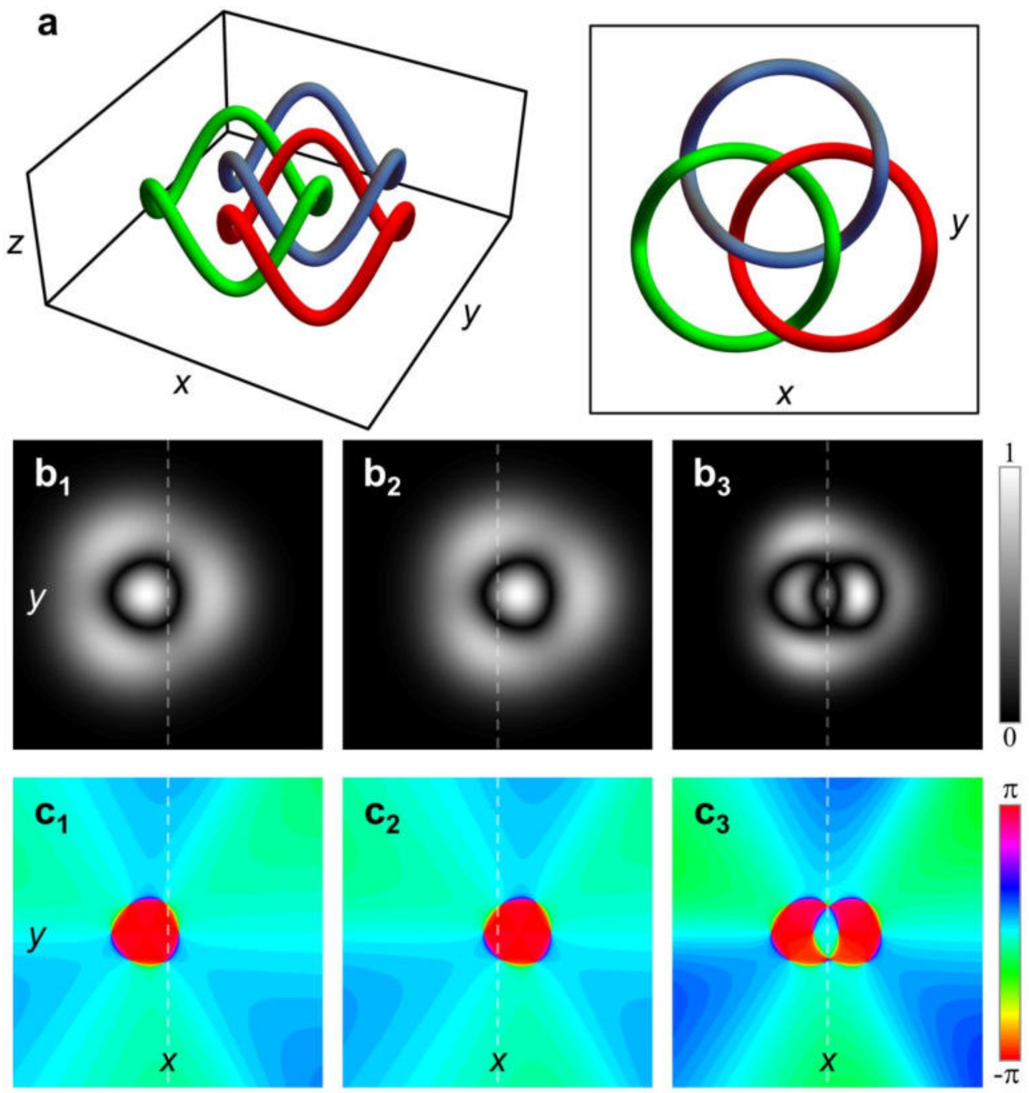

Figure S3. The strategy of constructing Borromean vortex ring using the isolated vortex ring. (a) 3D Borromean rings generated from the parametric equations. (b) amplitude and **c** phase of the topological light fields. (b_1, c_1) The light field after a shift along the negative *x*-axis; (b_2, c_2) The light field after a shift along the positive *x*-axis; (b_3, c_3) the product of the two fields.

References

(1) Allen, L.; Beijersbergen, M. W.; Spreeuw, R. J. C.; Woerdman, J. P. Orbital angular momentum of light and the transformation of Laguerre-Gaussian laser modes. *Phys. Rev. A* **1992**, 45 (11), 8185-8189.

(2) King, R. P., Knotting of optical vortices, (University of southampton, 2010).

(3) Zhong, J. and Zhan, Q. Structured Optical Toroidal Vortices with Rotational Symmetry. *Photonics* **2025**, 12 (3), 288.

(4) Kong, L.-J.; Zhang, W.; Li, P.; Guo, X.; Zhang, J.; Zhang, F.; Zhao, J.; Zhang, X. High capacity topological coding based on nested vortex knots and links. *Nat. Commun.* **2022**, 13, 2705.